



Exploring non standard interactions effects in T2HK and DUNE

Barnali Brahma^a , Anjan Giri^b

Department of Physics, Indian Institute of Technology Hyderabad, Kandi 502284, India

Received: 27 September 2022 / Accepted: 13 December 2022 / Published online: 19 December 2022
© The Author(s) 2022

Abstract Neutrino oscillations in matter offer a novel path to investigate new physics. One of the main goals of neutrino experiments is to determine the CP phase, and the presence of new physics can alter the scenario. We assume that the observed difference, if any, in the CP phase is due to the possible non-standard interactions. We derive the relevant coupling strengths using the results of NO ν A and T2K and study their effects in the next generation of long-baseline experiments: T2HK and DUNE. Our analysis reveals a significant impact on the sensitivity of atmospheric mixing angle θ_{23} in the normal and inverted orderings. Furthermore, we observe discernible differences in probabilities for both experiments when non-standard interaction from $e - \mu$ and $e - \tau$ sectors are included.

1 Introduction

Accelerator-based neutrino experiments offer exciting avenues to study neutrino physics. They travel long distances (a few hundred kilometers for the long baseline experiments currently underway) and are detected far from the source. Neutrinos change their flavor while going from one place to another and mix among the various mass eigenstates. Interestingly, neutrino oscillations [1, 2] provide us with indirect signature of physics beyond the standard model. On entering the Earth's atmosphere and travelling through the Earth's crust, the neutrino gets influenced by a matter potential known as the Wolfenstein matter effect. Wolfenstein in addition to the neutrino mass matrix [3], introduced non-standard interaction (NSI) to investigate new physics. There have been extensive studies of neutrino phenomenology in the literature [4–12]. NSI describes new physics models at low energies in which neutrino interactions with ordinary matter are param-

eterized in terms of effective coupling $\epsilon_{\alpha\beta}$ (defined later in the text) [13–29]. For the latest review on NSI and related work, one can see Ref. [30] and the references therein.

NSI effects can exhibit interesting signatures that can be differentiated from the standard model predictions and thus provide golden avenues to decipher new physics. NSI arises naturally from the high-energy physics of new heavy states [30–32] or light mediators [33–35]. It is quite crucial to comprehend how NSI affect standard neutrino oscillation in matter. However, in this article, we will not resort to any specific scenario but assume that new physics arises only from the NSI and is responsible for any deviation. In general, NSI affects neutrino propagation in matter not only through neutral-current interactions but also through charged-current interactions, which affect neutrino generation and detection. Neutral current NSI interacting with matter fields can yield observable effects. As model-independent bounds on the production and detection of NSI are typically orders of magnitude higher than those of matter NSI, we ignore the production and detection of NSI in this study and focus solely on NSI due to propagation.

The standard model (SM) CP phase promises to help us understand the baryon asymmetry of the universe and is the most sought-after observable in the currently running and future neutrino experiments. The most recent results from the two long-baseline accelerator experiments, NO ν A and T2K, show some kind of tension in the standard 3-flavor scenario. NO ν A detects neutrinos at the far detector, which is 810 km away from the source, with an energy of approximately 2 GeV. T2K detects neutrinos with an energy of 0.6 GeV at far detector, which is 295 km away from the source. Both NO ν A and T2K are off-axis experiments and they detect a stream of neutrinos with a very narrow energy distribution.

According to the recent results, NO ν A prefer the CP phase to be close to $\delta_{CP} \approx 0.8\pi$ [36] whereas T2K hints a value of δ_{CP} around 1.5π [37] in the case of normal ordering.

^a e-mail: ph19resch11001@iith.ac.in (corresponding author)

^b e-mail: giria@phy.iith.ac.in

There appears to be no disagreement in the case of inverted ordering. Once the NSI from the $e - \mu$ sector is taken into account the tension concerning the δ_{CP} parameter for NO ν A and T2K becomes placid, but one can see a difference for θ_{23} [38, 39]. NO ν A prefers lower octant, whereas T2K prefers higher octant. We extracted datasets of NO ν A [40] and T2K [41] from the recent data release in order to find the constraints on NSI contributions. Thereafter, we use the same coefficients to see if we can get any discernible result in future long-baseline (LBL) neutrino experiments, such as the DUNE and T2HK. In particular, T2HK, with its short baseline and low energy, will not be as sensitive to the matter effect as will be DUNE, with its relatively larger baseline and high energy. The objective here is to determine whether or not the degeneracy for the standard model parameter θ_{23} persists in the presence of NSI arising from both $e - \mu$ and $e - \tau$ sectors for DUNE and T2HK. In addition to that, we also explore the question of mass ordering through oscillation probability plots and sensitivity to the CP violating parameter δ_{CP} .

2 Formalism

The NSI can be characterised by six-dimensional four-fermion (ff) operators of the form [3]:

$$\mathcal{L}_{NSI} = 2\sqrt{2}G_F \epsilon_{\alpha\beta}^{fC} [\bar{\nu}_\alpha \gamma^\rho P_L \nu_\beta][\bar{f} \gamma_\rho P_C f] + h.c. \quad (1)$$

where $\alpha, \beta = e, \mu, \tau$ indicate the neutrino flavor, superscript $C = L, R$ refers to the chirality of ff current, $f = u, d, e$ denotes the matter fermions and $\epsilon_{\alpha\beta}^{fC}$ are dimensionless parameters that measure the new interaction's strength in relation to the SM. The neutrino propagation Hamiltonian in the presence of matter, NSI, can be expressed as

$$H_{Eff} = \frac{1}{2E} \left[U_{PMNS} \begin{bmatrix} 0 & 0 & 0 \\ 0 & \Delta m_{21}^2 & 0 \\ 0 & 0 & \Delta m_{31}^2 \end{bmatrix} U_{PMNS}^\dagger + V \right]$$

where U_{PMNS} is the unitary Potecorvo–Maki–Nakagawa–Sakata mixing matrix, E is the neutrino energy and $\Delta m_{21}^2 \equiv m_2^2 - m_1^2$, $\Delta m_{31}^2 \equiv m_3^2 - m_1^2$. m_1, m_2 and m_3 are the different mass eigenstates. V is written as:

$$V = 2\sqrt{2}G_F N_e E \begin{bmatrix} 1 + \epsilon_{ee} & \epsilon_{e\mu} e^{i\phi_{e\mu}} & \epsilon_{e\tau} e^{i\phi_{e\tau}} \\ \epsilon_{\mu e} e^{-i\phi_{e\mu}} & \epsilon_{\mu\mu} & \epsilon_{\mu\tau} e^{i\phi_{\mu\tau}} \\ \epsilon_{\tau e} e^{-i\phi_{e\tau}} & \epsilon_{\tau\mu} e^{-i\phi_{\mu\tau}} & \epsilon_{\tau\tau} \end{bmatrix}$$

N_e is the number density of electrons and for neutrino propagation in the Earth, G_F is Fermi coupling constant, $\epsilon_{\alpha\beta} e^{i\phi_{\alpha\beta}} \equiv \sum_{f,C} \epsilon_{\alpha\beta}^{fC} \frac{N_f}{N_e} \equiv \sum_{f=e,u,d} (\epsilon_{\alpha\beta}^{fL} + \epsilon_{\alpha\beta}^{fR}) \frac{N_f}{N_e}$, N_f being the number density of f fermion. The $\epsilon_{\alpha\beta}$ are real

and $\phi_{\alpha\beta} = 0$ for $\alpha = \beta$. We concentrate on flavour non-diagonal NSI ($\epsilon_{\alpha\beta}$'s with $\alpha \neq \beta$). Here, we consider single NSI parameter $\epsilon_{e\mu}$ or $\epsilon_{e\tau}$ (one at a time) to examine the conversion probability of $\nu_\mu \rightarrow \nu_e$ for the LBL studies which can be stated as the sum of three (plus higher order; cubic and beyond) terms in the presence of NSI [42–44]:

$$P_{\mu e} = P_0 + P_1 + P_2 + h.o. \quad (2)$$

the above Eq. (2), similar to [45] takes the following form:

$$P_0 = 4s_{13}^2 s_{23}^2 f^2 + 8s_{13}s_{23}s_{12}c_{12}c_{23}rfg \cos(\Delta + \delta_{CP}) + 4r^2 s_{12}^2 c_{12}^2 c_{23}^2 g^2$$

$$P_1 = 8\hat{A}\epsilon_{e\mu}[s_{13}s_{23}[s_{23}^2 f^2 \cos(\Psi_{e\mu}) + c_{23}^2 fg \cos(\Delta + \Psi_{e\mu})] + 8rs_{12}c_{12}c_{23}[c_{23}^2 g^2 \cos \Psi_{e\mu} + s_{23}^2 g \cos(\Delta - \phi_{e\mu})]]$$

and,

$$P_2 = 8\hat{A}\epsilon_{e\tau}[s_{13}c_{23}[s_{23}^2 f^2 \cos(\Psi_{e\tau}) - s_{23}^2 fg \cos(\Delta + \Psi_{e\tau})] - 8rs_{12}c_{12}s_{23}[c_{23}^2 g^2 \cos \Psi_{e\tau} - c_{23}^2 g \cos(\Delta - \phi_{e\tau})]]$$

where, $f \equiv \frac{\sin[(1-\hat{A})\Delta]}{1-\hat{A}}$; $g \equiv \frac{\sin \hat{A}\Delta}{\hat{A}}$; $\hat{A} = \frac{2\sqrt{2}G_F N_e E}{\Delta m_{31}^2}$; $\Delta = \frac{\Delta m_{31}^2 L}{4E}$; $r = \frac{\Delta m_{21}^2}{\Delta m_{31}^2}$. Furthermore, here we used: $\Psi_{e\mu} = \phi_{e\mu} + \delta_{CP}$; $\Psi_{e\tau} = \phi_{e\tau} + \delta_{CP}$.

3 Analysis details and results

In our analysis, we used the software GLoBES [46, 47] and its additional public tool [48]. The best fit values of the standard model parameters along with their corresponding uncertainties are taken from nuFIT v5.1 [49] and PDG [50]. For example, the parameter values taken (for normal ordering) are: $\sin^2 \theta_{12} = 0.304_{-0.012}^{+0.013}$; $\sin^2 \theta_{23} = 0.573_{-0.023}^{+0.018}$; $\sin^2 \theta_{13} = 0.02220_{-0.00062}^{+0.00068}$; $\delta_{CP} = 194_{-25}^{+52}$; $\frac{\Delta m_{31}^2}{10^{-5} eV^2} = 7.42_{-0.20}^{+0.21}$; and $\frac{\Delta m_{21}^2}{10^{-3} eV^2} = +2.517_{-0.028}^{+0.028}$. We utilised GLoBES to combine the extracted datasets of T2K and NO ν A. Using the obtained NSI constraints we discuss the sensitivity as well as the oscillation probabilities for the two next generation LBL experiments: DUNE and T2HK. We used the AEDL (a comprehensive abstract experiment definition language) files available for simulating experiments like T2HK and DUNE [51]. For our analysis purpose, we used DUNE and T2HK running for 3.5 years and 3 years in ν mode and similarly 3.5 years and 4 years in $\bar{\nu}$ mode, respectively.

In the case of DUNE, it will have a 40 kiloton liquid argon detector that will use a 1.2 MW proton beam to generate neutrino and antineutrino beams from in-flight pion decays. The proton beam will originate 1300 km upstream at Fermilab. The neutrino energy ranges will be between 0.5 and 20 GeV

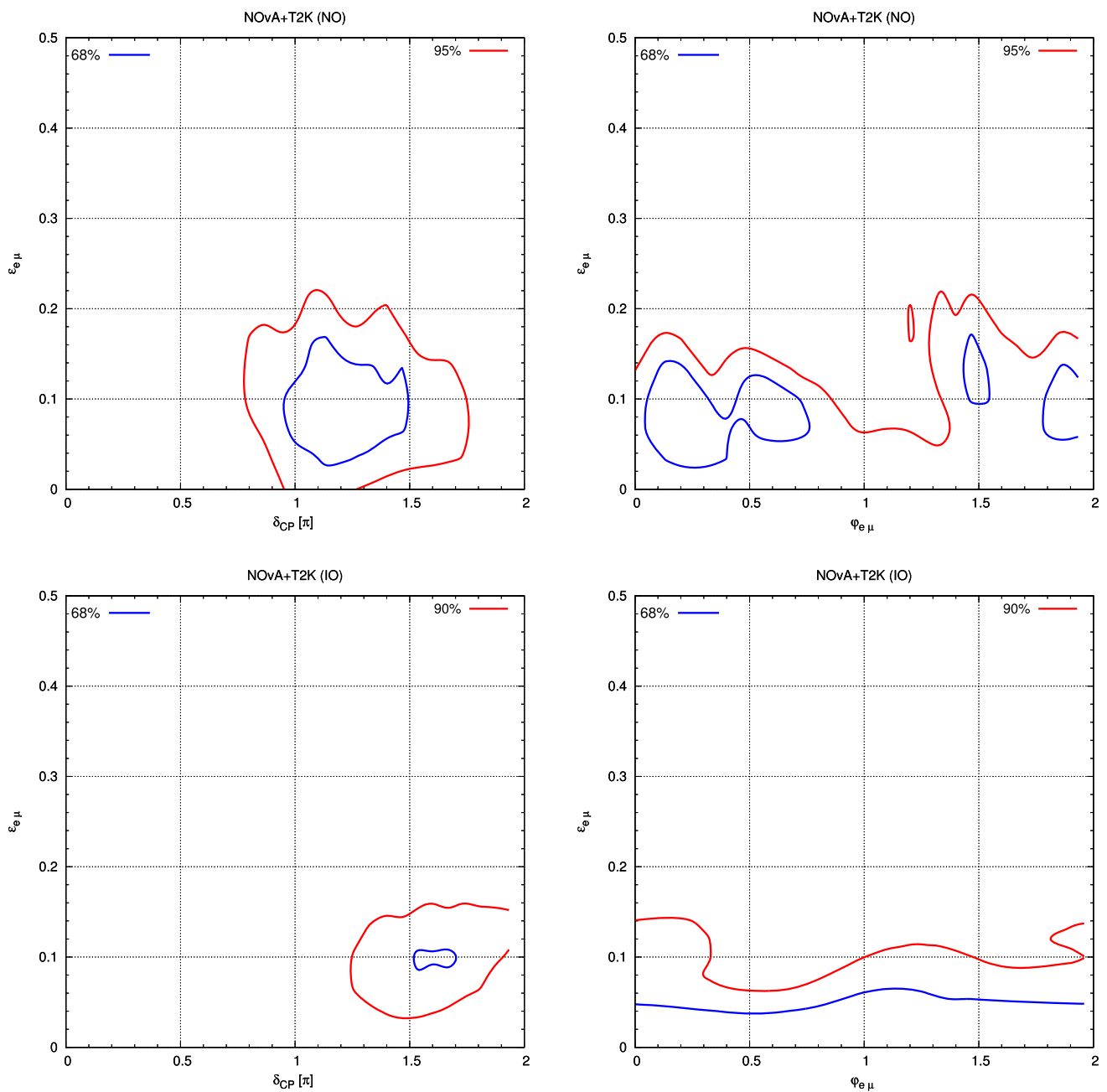


Fig. 1 Allowed regions for $\epsilon_{e\mu}$ and the CP phase (left); $\epsilon_{e\mu}$ and phase $\phi_{e\mu}$ (right) determined by the combination of T2K and NOvA for NO (top panel) and IO (bottom panel). The contours are drawn at the 68% and 90% C.L. for 2 d.o.f

and the flux peak around 3.0 GeV. Whereas, T2HK experiment will have a 225 kt water Cherenkov detector. It will use an upgraded 30 GeV J-PARC beam with a power of 1.3 MW and its detector will be located 295 km away from the source.

In Fig. 1 (top panel), the results of the analysis for the combination of T2K and NOvA are displayed. The left panel shows the allowed region in the plane spanned by $\epsilon_{e\mu}$ and the CP-phase δ_{CP} , whereas the right panel displays the allowed region for $\epsilon_{e\mu}$ and the NSI phase $\phi_{e\mu}$. For the left panel plot

the non-standard CP-phase $\phi_{e\mu}$, θ_{13} , and θ_{23} are marginalized away whereas for the right panel plot θ_{13} , θ_{23} , and δ_{CP} are marginalized. The similar plots for IO case are displayed in Fig. 1 (bottom panel)

Similarly, in Fig. 2, the left panel shows the allowed region in the plane spanned by $\epsilon_{e\tau}$ and the CP-phase δ_{CP} , whereas the right panel displays the allowed region for $\epsilon_{e\tau}$ and the NSI phase $\phi_{e\tau}$. For the left panel plot, the non-standard CP-phase $\phi_{e\tau}$, θ_{13} , and θ_{23} are marginalized away whereas for the right panel plot θ_{13} , θ_{23} , and δ_{CP} are marginalized.

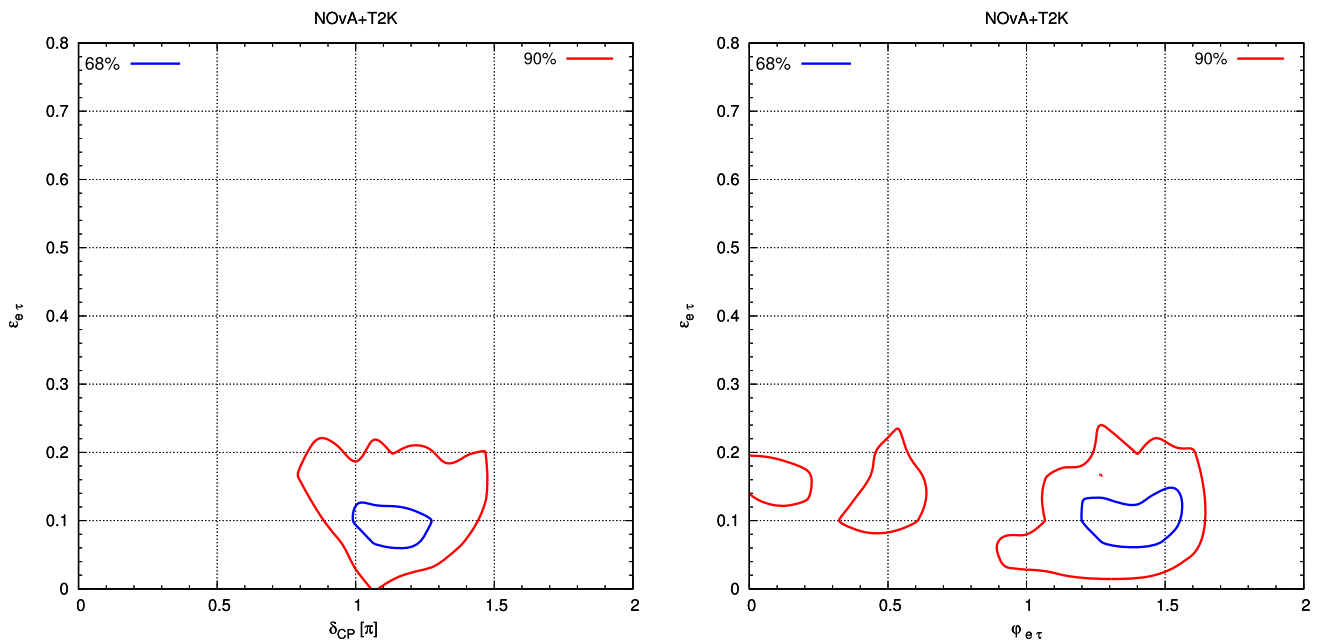


Fig. 2 Allowed regions for coupling $\epsilon_{e\tau}$ and CP phase (left); $\epsilon_{e\tau}$ and phase $\phi_{e\tau}$ (right) determined by the combination of T2K and NO ν A for NO. The contours are drawn at the 68% and 90% C.L. for 2 d.o.f

Table 1 From allowed region plots, the best fit points are listed here. The best fit points are picked up corresponding to the minimum χ^2 value. These values are also included in the below table

Mass ordering	NSI	$ \epsilon_{\alpha\beta} $	$\phi_{\alpha\beta}/\pi$	χ^2
NO	$\epsilon_{e\mu}$	0.1	0.2	0.518
	$\epsilon_{e\tau}$	0.1	1.47	0.385
IO	$\epsilon_{e\mu}$	0.01	1.67	0.533
	$\epsilon_{e\tau}$	0.13	0.8	1.668

From the right panel of Figs. 1 and 2 we can visualize that both in NO as well as in IO cases there is a preference for a non-zero value of the coupling $|\epsilon_{e\mu}|$ and $|\epsilon_{e\tau}|$ and their corresponding phases $\phi_{e\mu}$ and $\phi_{e\tau}$, whose values are listed out in Table 1. These values are consistent with the global constraints on neutral current NSI parameters [52]. We found δ_{CP} value for $e - \mu$ sector around 1.12π (for NO case) as evident from the top left panel of Fig. 1. Interestingly, for $e - \tau$ sector we obtained similar value of δ_{CP} (Fig. 2).

In Fig. 3 (top panel), we display the allowed regions in the plane spanned by the standard CP-phase δ_{CP} and the atmospheric mixing angle θ_{23} in the NO case for DUNE. The left panel refers to the SM case, while the middle and right panels concern the SM+NSI scenario with NSI arising from the $e - \mu$ and $e - \tau$ sectors, respectively. The mixing angle θ_{13} and Δm_{31}^2 are marginalized away in the SM case whereas along with θ_{13} and Δm_{31}^2 relevant NSI coupling ($\epsilon_{e\mu}/\epsilon_{e\tau}$) and non-standard CP-phase ($\phi_{e\mu}/\phi_{e\tau}$) are marginalized in SM+NSI case. In the middle and right panels we have taken the NSI parameters with their best fit values from the combined analysis of NO ν A and T2K. More specifically, $|\epsilon_{e\mu}| =$

0.1, $\phi_{e\mu} = 0.2\pi$ (middle panel) and $|\epsilon_{e\tau}| = 0.1$, $\phi_{e\tau} = 1.47\pi$ (right panel).

In Fig. 3 (bottom panel), similarly, we display the allowed regions in the plane spanned by the standard CP-phase δ_{CP} and the atmospheric mixing angle θ_{23} in the NO case but now for T2HK. The left panel refers to the SM case, while the middle and right panels concern the SM+NSI scenario with NSI from the $e - \mu$ and $e - \tau$ sectors, respectively. Comparing the SM scenario with that of SM+NSI arising from $e - \mu$ sector, we found distinct parameter space in the determination of θ_{23} for both DUNE and T2HK. When NSI is included with SM, the allowed region corresponding to the higher octant disappears and we are left only with the allowed region from the lower octant. Whereas in SM+NSI scenario from $e - \tau$ sector, we find that both the lower as well as the higher octants are allowed for T2HK and DUNE with increased parameter space.

Concerning the θ_{23} octant, we note that in the SM and SM+NSI case arising from $e - \mu$ sector there is a clear preference for lower octant for DUNE ($\Delta\chi^2 = 3.69$) and similarly for T2HK ($\Delta\chi^2 = 0.81$), where $\Delta\chi^2 = \chi_{SM}^2 - \chi_{SM+NSI}^2$. Corresponding one-dimensional projection plots are given in

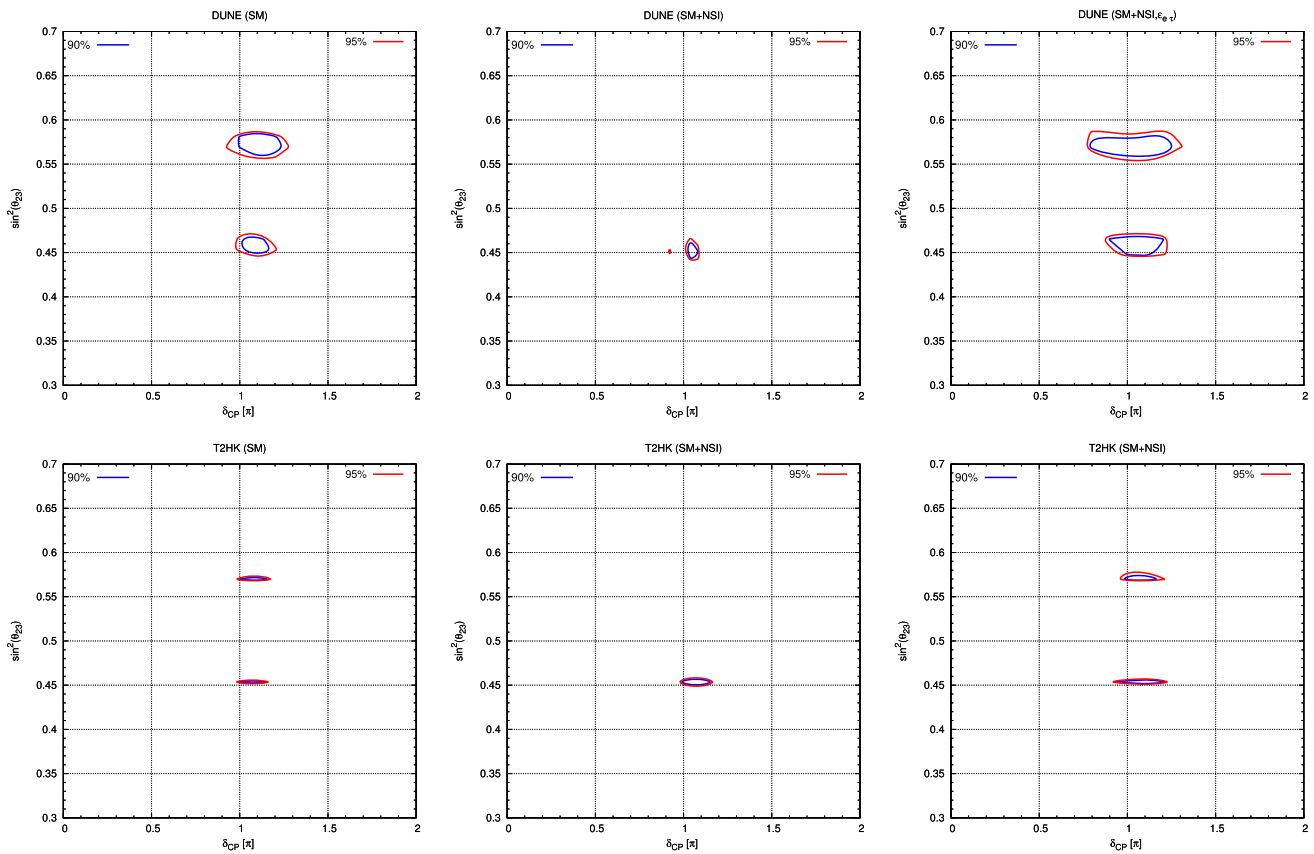


Fig. 3 Allowed regions determined separately by DUNE and T2HK for NO in the SM case (left panel) and with NSI in the $e - \mu$ sector (middle panel) and in the $e - \tau$ sector (right panel). In the middle panel we have taken the NSI parameters at their best fit values of $\text{NO}\nu\text{A}+\text{T2K}$

($|\epsilon_{e\mu}| = 0.1, |\phi_{e\mu}| = 0.2\pi$). Similarly, in the right panel we have taken $|\epsilon_{e\tau}| = 0.1, |\phi_{e\tau}| = 1.47\pi$. The contours are drawn at the 90% and 95% C.L. for 2 d.o.f

Figs. 4 and 5. Similar exercise for IO is also carried out and the conclusions follow similar pattern like the NO results.

4 Effect of NSI parameters on oscillation probability

In order to understand clearly the effect of NSI on LBL experiments, DUNE and T2HK, we discuss next the corresponding probability plots for both neutrino and anti-neutrino modes.

In Fig. 6 (top panel), the oscillation probability plots for DUNE in neutrino mode in the SM (left panel), SM+NSI from the $e - \mu$ sector (middle panel), and SM+NSI from the $e - \tau$ sector (right panel) are shown. We see a good separation between NO–IO for both $\delta_{CP} = 90^\circ$ and $\delta_{CP} = -90^\circ$ in the SM scenario. For SM+NSI scenario from the $e - \mu$ sector, we still have some separation between NO–IO for $\delta_{CP} = 90^\circ$ in mid energy region, and they gradually merges around 4 GeV. Whereas $\delta_{CP} = -90^\circ$ has good NO–IO separation. For SM+NSI scenario from the $e - \tau$ sector, we see a reasonable separation between NO–IO for $\delta_{CP} = 90^\circ$. In the case of $\delta_{CP} = -90^\circ$, there is some NO–IO separation

in mid energy region, which gradually decreases as energy increases.

The oscillation probability plots for T2HK in neutrino mode in the SM (left panel), SM+NSI from the $e - \mu$ sector (middle panel) and SM+NSI from the $e - \tau$ sector (right panel) are shown in Fig. 7. We see a perceptible separation between NO–IO for both $\delta_{CP} = 90^\circ$ and $\delta_{CP} = -90^\circ$ until 1 GeV energy in the SM scenario. For the SM+NSI case from $e - \mu$ sector, we see a better separation between NO–IO for $\delta_{CP} = -90^\circ$. The NO–IO separation continuously decreases for $\delta_{CP} = 90^\circ$ crossing each other around 0.7 GeV. For the SM+NSI case, from $e - \tau$ sector, we see a separation between NO–IO for $\delta_{CP} = 90^\circ$ until 1.5 GeV, whereas there is no NO–IO separation for $\delta_{CP} = -90^\circ$ after 0.7 GeV energy. We have repeated the exercise for anti-neutrino case in DUNE displayed in Fig. 6 (bottom panel) and find similar striking differences for NO–IO.

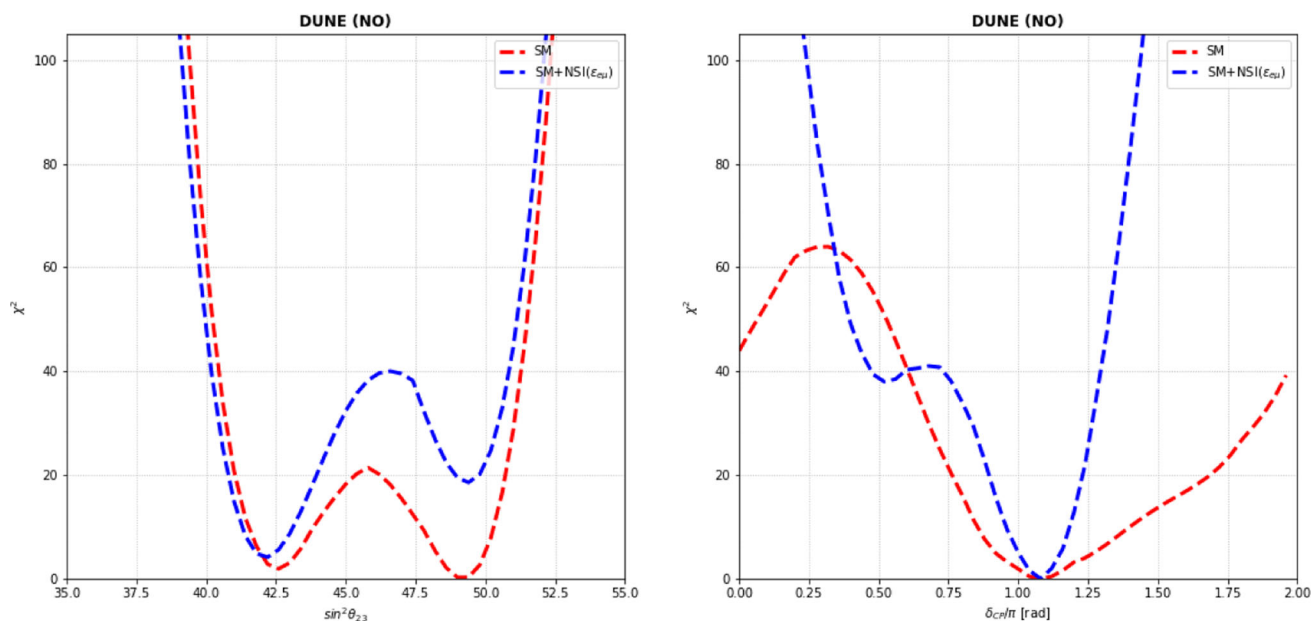


Fig. 4 One-dimensional projections of the standard parameters θ_{23} (left) and δ_{CP} (right) determined for DUNE in NO for SM (red dashed curves) and SM+NSI from $e - \mu$ scenario (blue dashed curves)

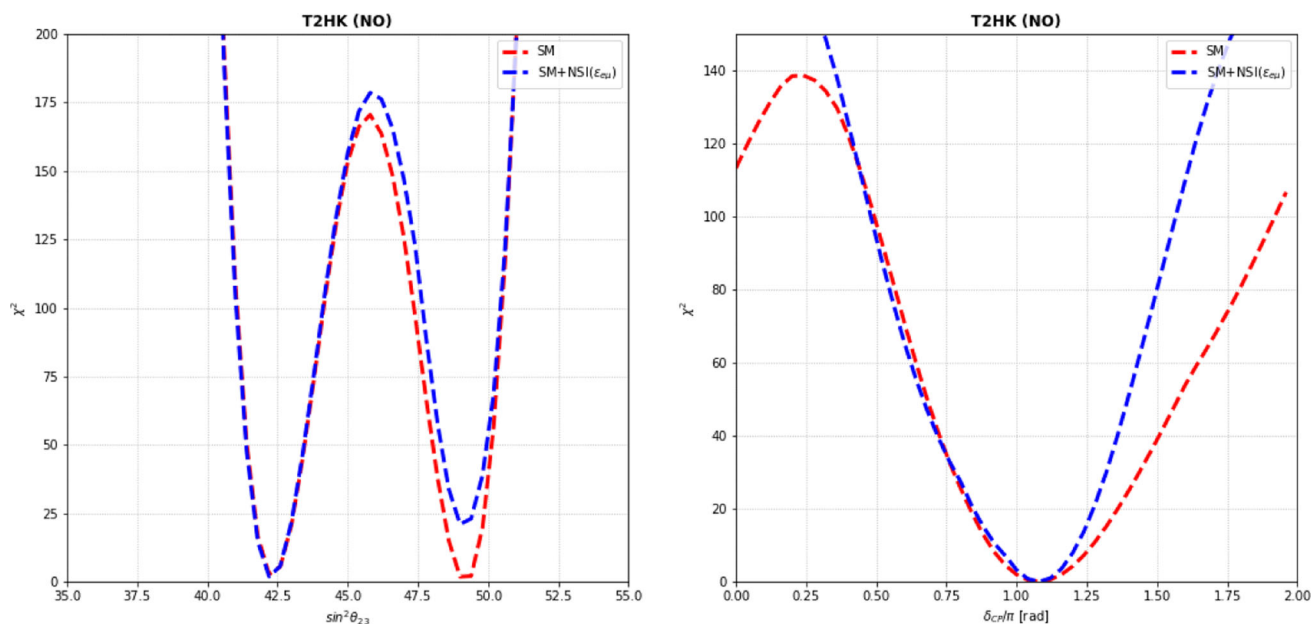


Fig. 5 One-dimensional projections of the standard parameters θ_{23} (left) and δ_{CP} (right) determined for T2HK in NO for SM (red dashed curves) and SM+NSI from $e - \mu$ scenario (blue dashed curves)

5 CP violation sensitivity

As mentioned before, one of important objectives of the current and future LBL neutrino experiments is to determine the CP phase δ_{CP} , as precisely as possible. In the standard framework of three neutrino oscillation, we discuss here about CP violation sensitivity. The signal indicating CP violation in the lepton sector will be seen if the true values of δ_{CP} dif-

fers from the CP conserving values by a considerable amount [53]. Here,

$$\Delta\chi_{CPV}^2 = \text{Min}[\Delta\chi_{CP}^2(\delta_{CP}^{test} = 0), \Delta\chi_{CP}^2(\delta_{CP}^{test} = \pi)]$$

We found that for both DUNE and T2HK in Fig. 8 there is appreciable difference in the sensitivities for SM+NSI case

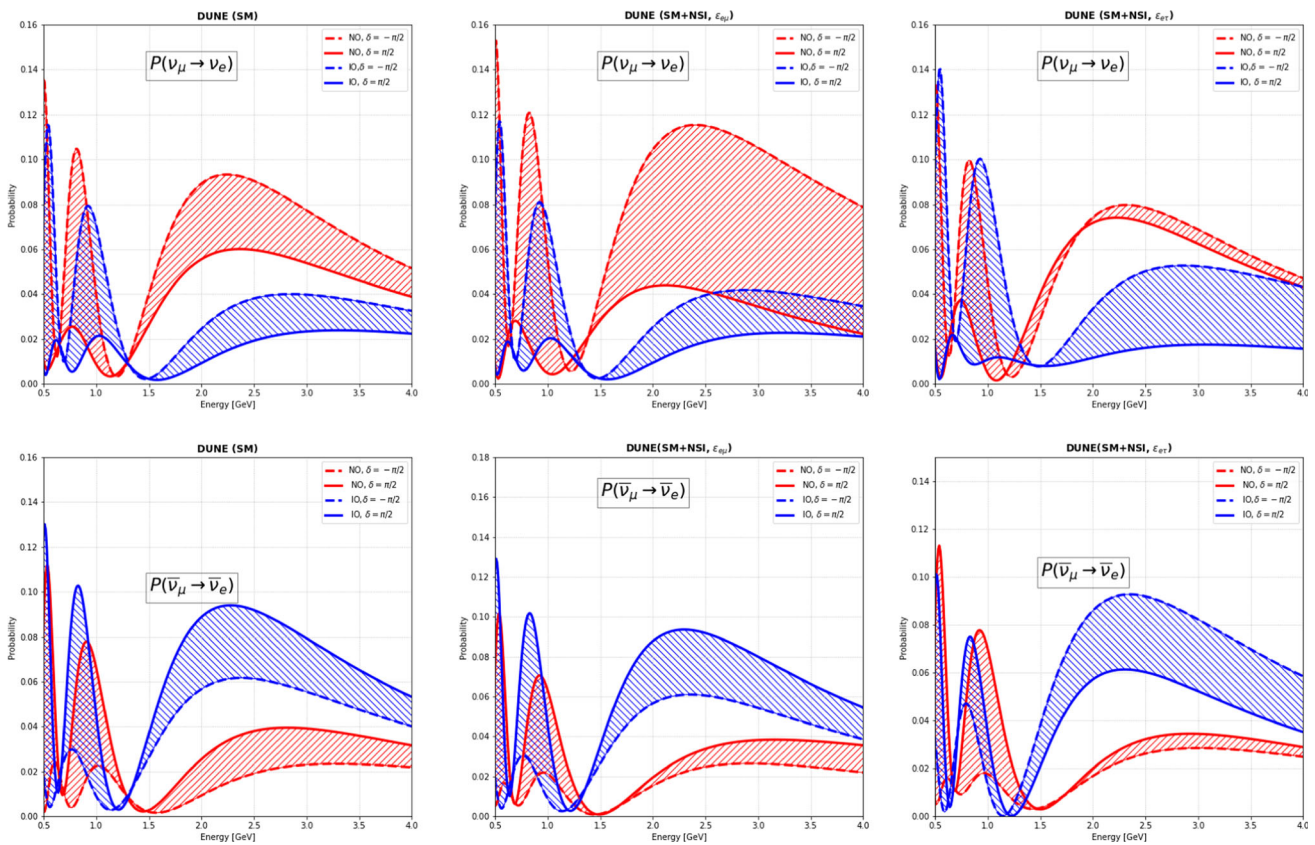


Fig. 6 Probability Plots for DUNE in SM (left) and SM+NSI scenario with NSI arising from $e - \mu$ sector (middle) and $e - \tau$ sector (right) for ν (top panel) and $\bar{\nu}$ (bottom panel) mode

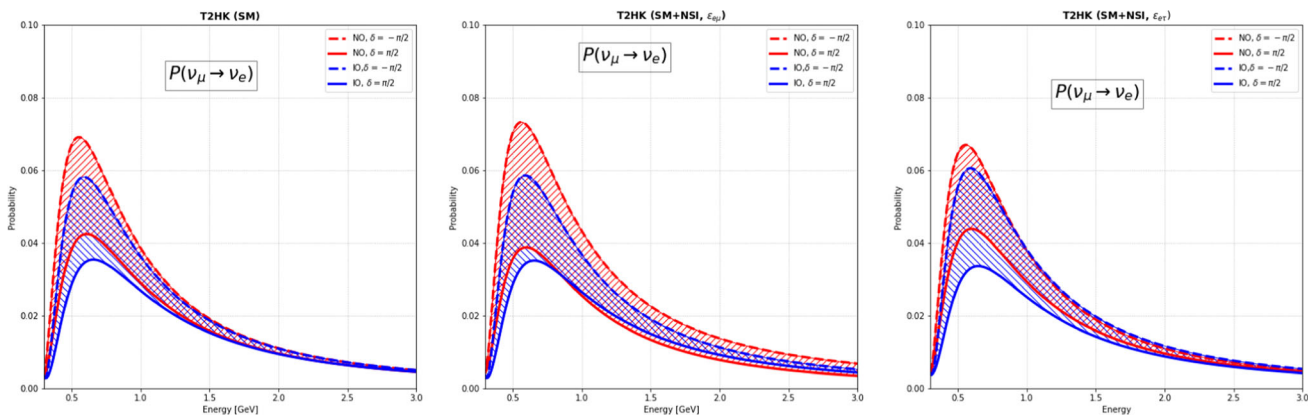


Fig. 7 Probability plots for T2HK in SM (left) and SM+NSI scenario with NSI arising from $e - \mu$ sector (middle) and $e - \tau$ sector (right)

in comparison to SM prediction. In the case of the DUNE there appears to be better sensitivity to NSI than T2HK.

6 Conclusions

In this article, we assumed that new physics occurs in the form of NSI. Following that, we obtained the constraints on NSI parameters by combining the $\text{NO}\nu\text{A}$ and T2K datasets.

We used the derived constraints (we have considered here mostly the case for normal ordering but checked that similar results also follow in the case of inverted ordering) and have shown that for θ_{23} when we use NSI arising from the $e - \mu$ sector, both DUNE and T2HK prefer the lower octant, whereas inclusion of NSI arising from the $e - \tau$ sector brings back the degeneracy of both the lower and higher octants. Moreover, using the same set of constraints, we see striking differences in oscillation probabilities for both neutrino and

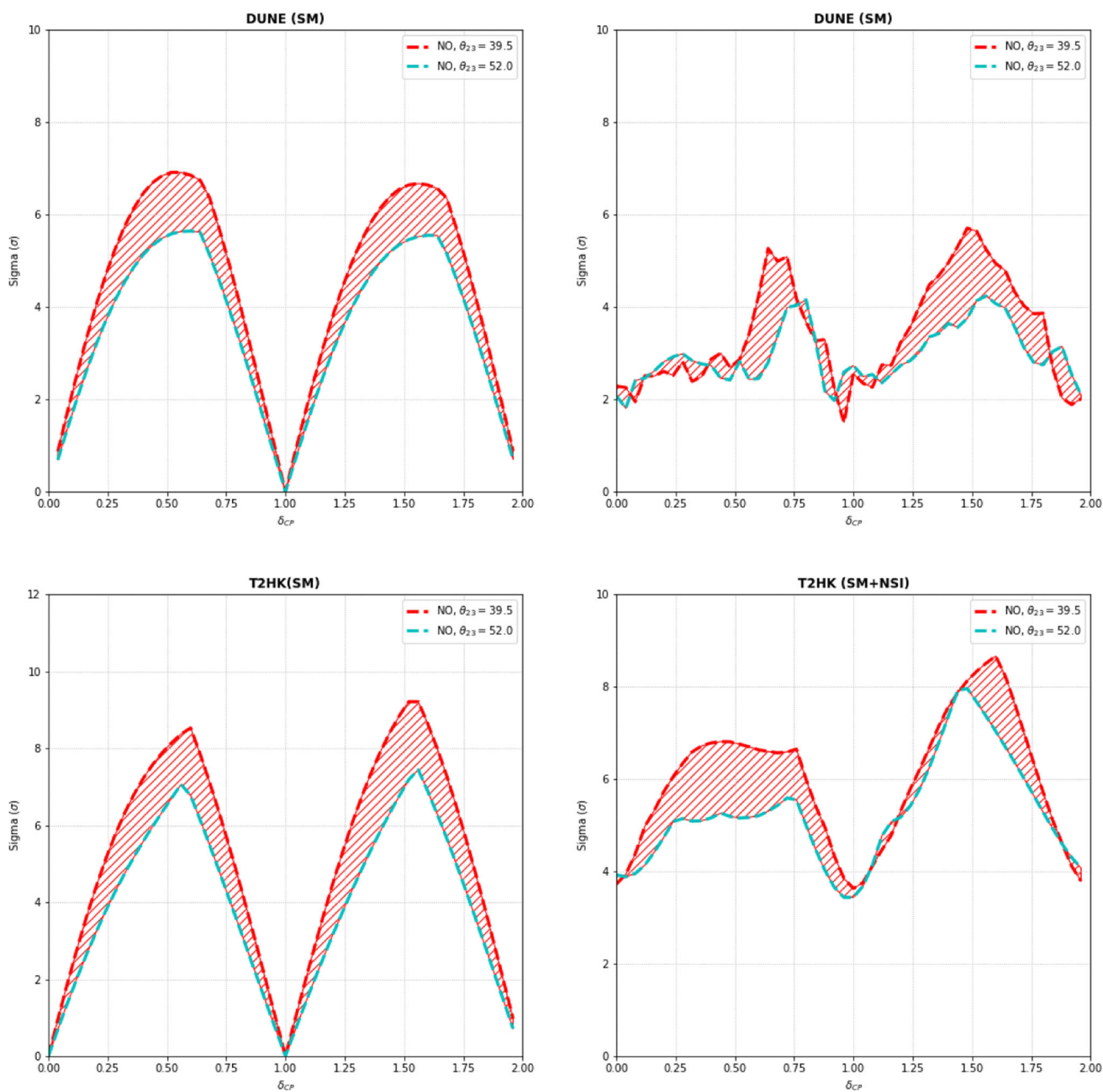


Fig. 8 CP discovery potential for DUNE (top panel) and T2HK (bottom panel) as a function of the true value of the leptonic CP phase for NO in SM scenario (left panel) and SM+NSI scenario (right panel). The bands represent the range in sensitivity obtained under the two different assumption of θ_{23} value

anti-neutrino channels in DUNE and T2HK, which can help us understand the neutrino mass ordering problem. Furthermore, we have shown the CP discovery potential for both SM and SM+NSI scenarios and observed that the effect of NSI reduces the sensitivity, which is prominent in DUNE. Future data from NO ν A and T2K will determine the fate of the existing tension in δ_{CP} and clear the picture. If the tension persists, as we have shown in this analysis, it could probably signal the existence of new physics. Nonetheless,

future studies may enable us to disentangle the NSI effects for cleaner extraction of the neutrino parameters.

Acknowledgements We are greatly indebted to Dr. Sabyasachi Chatterjee for the valuable correspondence. The authors also acknowledge the support from the DST, India under project No. SR/MF/PS-01/2016-IITH/G and fellowship from MoE, India.

Data Availability Statement This manuscript has no associated data or the data will not be deposited. [Authors' comment: We have used GLOBES simulation and published datasets of NO ν A and T2K.]

Open Access This article is licensed under a Creative Commons Attribution 4.0 International License, which permits use, sharing, adaptation, distribution and reproduction in any medium or format, as long as you give appropriate credit to the original author(s) and the source, provide a link to the Creative Commons licence, and indicate if changes were made. The images or other third party material in this article are included in the article's Creative Commons licence, unless indicated otherwise in a credit line to the material. If material is not included in the article's Creative Commons licence and your intended use is not permitted by statutory regulation or exceeds the permitted use, you will need to obtain permission directly from the copyright holder. To view a copy of this licence, visit <http://creativecommons.org/licenses/by/4.0/>.

Funded by SCOAP³. SCOAP³ supports the goals of the International Year of Basic Sciences for Sustainable Development.

References

1. Y. Fukuda et al., Super-Kamiokande. *Phys. Rev. Lett.* **81**, 1562 (1998). [arXiv:hep-ex/9807003](https://arxiv.org/abs/hep-ex/9807003)
2. Q.R. Ahmad et al. [SNO Collaboration], *Phys. Rev. Lett.* **89**, 011302 (2002)
3. L. Wolfenstein, *Phys. Rev. D* **17**, 2369 (1978)
4. R. Davis Jr., D.S. Harmer, K.C. Hoffman, *Phys. Rev. Lett.* **20**, 1205 (1968)
5. P. Minkowski, *Phys. Lett. B* **67**, 421 (1977)
6. R.N. Mohapatra, G. Senjanovic, *Phys. Rev. Lett.* **44**, 912 (1980)
7. M.M. Guzzo, A. Masiero, S.T. Petcov, *Phys. Lett. B* **260**, 154 (1991)
8. M.C. Gonzalez-Garcia, M.M. Guzzo, P.I. Krastev, H. Nunokawa, O.L.G. Peres, V. Pleitez, J.W.F. Valle, R. Zukanovich Funchal, *Phys. Rev. Lett.* **82**, 3202 (1999). [arXiv:hep-ph/9809531](https://arxiv.org/abs/hep-ph/9809531)
9. A. Friedland, C. Lunardini, *Phys. Rev. D* **72**, 053009 (2005). [arXiv:hep-ph/0506143](https://arxiv.org/abs/hep-ph/0506143)
10. O.G. Miranda, M.A. Tortola, J.W.F. Valle, *JHEP* **10**, 008 (2006). [arXiv:hep-ph/0406280](https://arxiv.org/abs/hep-ph/0406280)
11. P.A.N. Machado, H. Nunokawa, R. Zukanovich Funchal, *Nucl. Phys. B Proc. Suppl.* **217**, 357 (2011)
12. I. Esteban, M.C. Gonzalez-Garcia, M. Maltoni, T. Schwetz, A. Zhou, *JHEP* **09**, 178 (2020)
13. V.D. Barger, R.J.N. Phillips, K. Whisnant, *Phys. Rev. D* **44**, 1629 (1991)
14. Y. Grossman, *Phys. Lett. B* **359**, 141 (1995)
15. M.C. Gonzalez-Garcia, M. Maltoni, J. Salvado, *JHEP* **05**, 075 (2011). [arXiv:1103.4365](https://arxiv.org/abs/1103.4365) [hep-ph]
16. P. Huber, J.W.F. Valle, *Phys. Lett. B* **523**, 151 (2001). [arXiv:hep-ph/0108193](https://arxiv.org/abs/hep-ph/0108193)
17. N. Fornengo, M. Maltoni, R. Tomas, J.W.F. Valle, *Phys. Rev. D* **65**, 013010 (2002). [arXiv:hep-ph/0108043](https://arxiv.org/abs/hep-ph/0108043)
18. A. Palazzo, J.W.F. Valle, *Phys. Rev. D* **80**, 091301 (2009). [arXiv:0909.1535](https://arxiv.org/abs/0909.1535) [hep-ph]
19. P. Coloma, A. Donini, J. Lopez-Pavon, H. Minakata, *JHEP* **08**, 036. [arXiv:1105.5936](https://arxiv.org/abs/1105.5936) [hep-ph]
20. A. Esmaili, A.Y. Smirnov, *JHEP* **06**, 026 (2013)
21. P. Adamson et al. [MINOS], *Phys. Rev. D* **88**, 072011 (2013). [arXiv:1303.5314](https://arxiv.org/abs/1303.5314) [hep-ex]
22. S. Choubey et al., *JHEP* **12**, 126 (2015)
23. O.G. Miranda, H. Nunokawa, *New J. Phys.* **17**, 095002 (2015). [arXiv:1505.06254](https://arxiv.org/abs/1505.06254) [hep-ph]
24. P. Bakhti, Y. Farzan, *JHEP* **07**, 109 (2016)
25. R. Abbasi et al. [IceCube Collaboration], *Phys. Rev. D* **104**, 072006 (2021). [arXiv:2106.07755](https://arxiv.org/abs/2106.07755)
26. F. Capozzi, G.L. Fogli, E. Lisi, A. Marrone, D. Montanino, A. Palazzo, *Phys. Rev. D* **89**, 093018 (2014)
27. D.V. Forero, M. Tortola, J.W.F. Valle, *Phys. Rev. D* **90**, 093006 (2014). [arXiv:1405.7540](https://arxiv.org/abs/1405.7540) [hep-ph]
28. K.S. Babu, P.S. Dev, S. Jana, Y. Sui, *Phys. Rev. Lett.* **124**, 041805 (2020). [arXiv:1908.02779](https://arxiv.org/abs/1908.02779) [hep-ph]
29. R. Majhi, D.K. Singha, K.N. Deepthi, R. Mohanta (2022). [arXiv:2205.04269](https://arxiv.org/abs/2205.04269) [hep-ph]
30. P.S. Dev et al., Neutrino Non-Standard Interactions: A Status Report **2**, 001 (2019). [arXiv:1907.00991](https://arxiv.org/abs/1907.00991)
31. C. Biggio, M. Blennow, E. Fernandez-Martinez, *JHEP* **08**, 090. [arXiv:0907.0097](https://arxiv.org/abs/0907.0097) [hep-ph]
32. T. Ohlsson, *Rep. Prog. Phys.* **76**, 044201 (2013)
33. Y. Farzan, I.M. Shoemaker, *JHEP* **07**, 033
34. Y. Farzan, M. Tortola, *Front. Phys.* **6**, 10 (2018)
35. Y. Farzan, M. Lindner, W. Rodejohann, X.-J. Xu, *JHEP* **05**, 066. [arXiv:1802.05171](https://arxiv.org/abs/1802.05171) [hep-ph]
36. M.A. Acero et al. [NOvA] (2021). [arXiv:2108.08219](https://arxiv.org/abs/2108.08219) [hep-ex]
37. K. Abe et al. [T2K], *Phys. Rev. D* **103**, 112008 (2021)
38. S.S. Chatterjee, A. Palazzo, *Phys. Rev. Lett.* **126**, 051802 (2021). [arXiv:2008.04161](https://arxiv.org/abs/2008.04161) [hep-ph]
39. P.B. Denton, J. Gehrlein, R. Pestes, *Phys. Rev. Lett.* **126**, 051801 (2021). [arXiv:2008.01110](https://arxiv.org/abs/2008.01110) [hep-ph]
40. A. Himmel, Talk presented at neutrino 2020, 22 Jun 2020–Jul 2020, virtual meeting (2020)
41. P. Dunne, Talk presented at neutrino 2020, 22 Jun 2020–2 Jul 2020, virtual meeting (2020)
42. J. Kopp, M. Lindner, T. Ota, J. Sato, *Phys. Rev. D* **77**, 013007 (2008). [arXiv:0708.0152](https://arxiv.org/abs/0708.0152) [hep-ph]
43. T. Kikuchi, H. Minakata, S. Uchinami, *JHEP* **03**, 114. [arXiv:0809.3312](https://arxiv.org/abs/0809.3312) [hep-ph]
44. D. Meloni, T. Ohlsson, H. Zhang, *JHEP* **04**, 033. [arXiv:0901.1784](https://arxiv.org/abs/0901.1784) [hep-ph]
45. J. Liao, D. Marfatia, K. Whisnant, *Phys. Rev. D* **93**, 093016 (2016). [arXiv:1601.00927](https://arxiv.org/abs/1601.00927) [hep-ph]
46. P. Huber, J. Kopp, M. Lindner, M. Rolinec, W. Winter, *Comput. Phys. Commun.* **177**, 432 (2007). [arXiv:hep-ph/0701187](https://arxiv.org/abs/hep-ph/0701187)
47. P. Huber, M. Lindner, W. Winter, *Comput. Phys. Commun.* **167**, 195 (2005). [arXiv:hep-ph/0407333](https://arxiv.org/abs/hep-ph/0407333)
48. J. Kopp, <https://www.mpi-hd.mpg.de/personalhomes/globes/tools/snu-1.0.pdf> (2010)
49. <http://www.nufit.org/> (2021)
50. R.L. Workman et al. [Particle Data Group], *Rev. Part. Phys. PTEP* **2022**, 083C01 (2022)
51. <https://www.mpi-hd.mpg.de/personalhomes/globes/experiments.html>
52. P. Coloma, I. Esteban, M.C. Gonzalez-Garcia, M. Maltoni, *JHEP* **02**, 023 [Addendum: *JHEP* **12**, 071 (2020)]. [arXiv:1911.09109](https://arxiv.org/abs/1911.09109) [hep-ph]
53. D. Meloni, *JHEP* **08**, 028. [arXiv:1805.01747](https://arxiv.org/abs/1805.01747) [hep-ph]